

Negative conductivity and anomalous screening in two-dimensional electron systems subjected to microwave radiation

S. I. Dorozhkin,¹ I. A. Dmitriev,^{2,3} and A. D. Mirlin^{2,4,5}

¹*Institute of Solid State Physics, Chernogolovka, Moscow district, 142432, Russia*

²*Institut für Nanotechnologie, Karlsruhe Institute of Technology, 76021 Karlsruhe, Germany*

³*Ioffe Physical Technical Institute, 194021 St. Petersburg, Russia*

⁴*Institut für Theorie der kondensierten Materie and DFG Center for Functional Nanostructures, Karlsruhe Institute of Technology, 76128 Karlsruhe, Germany*

⁵*Petersburg Nuclear Physics Institute, 188300 St. Petersburg, Russia*

(Dated: July 28, 2018)

A 2D electron system in a quantized magnetic field can be driven by microwave radiation into a non-equilibrium state with strong magnetooscillations of the dissipative conductivity. We demonstrate that in such system a negative conductivity can coexist with a positive diffusion coefficient. In a finite system, solution of coupled electrostatic and linear transport problems shows that the diffusion can stabilize a state with negative conductivity. Specifically, this happens when the system size is smaller than the absolute value of the non-equilibrium screening length that diverges at the point where the conductivity changes sign. We predict that a negative resistance can be measured in such a state. Further, for a non-zero difference between the work functions of two contacts, we explore the distribution of the electrostatic potential and of the electron density in the sample. We show that in the diffusion-stabilized regime of negative conductivity the system splits into two regions with opposite directions of electric field. This effect is a precursor of the domain structure that has been predicted to emerge spontaneously in the microwave-induced zero-resistance states.

PACS numbers: 73.50.Pz, 73.43.Qt, 73.50.Fq, 73.50.Jt

I. INTRODUCTION

High mobility two-dimensional electron systems (2DES) subjected to the microwave radiation reveal giant magnetooscillations in the diagonal resistance ρ_{xx} ^{1,2} with periodicity controlled by the positions of the cyclotron resonance harmonics. In high-quality samples, these oscillations give rise to zero resistance states³⁻⁵ (ZRS) at the oscillation minima, $\rho_{xx} \rightarrow 0$, when the radiation power is increased and the temperature is lowered. In the Corbino-disk geometry ZRS manifest themselves as zero-conductance states. The widely accepted explanation of ZRS combines two distinct phenomena. The first one is development of the giant magnetoresistance oscillations due to indirect optical transitions⁶⁻⁸ or nonequilibrium occupation of electronic states⁹⁻¹¹. Both mechanisms predict, under appropriate conditions, a negative resistivity value in the oscillation minima at a small dc current. At some finite current density j_0 , the resistivity crosses zero and becomes positive^{8,11,12}. The second effect invoked for explanation of ZRS is spontaneous formation of current domains with current density j_0 ¹² which occurs due to instability of systems with negative absolute and/or differential resistivity¹²⁻¹⁴. In the simplest geometry the system breaks into two domains carrying equal Hall currents of opposite direction. The Hall electric fields related to these currents are also equal in magnitude and have opposite directions. The resulting dissipative component of the resistivity or conductivity tensor is zero¹². Two works^{15,16} provided an experimental evidence supporting the spontaneous domain formation in ZRS.

In this paper we show that a positive diffusion coefficient can stabilize a homogeneous state of a *finite* 2DES even though the system has a negative resistivity. We point out that combination of a negative resistivity and a positive diffusion coefficient naturally arises in 2DES under microwave radiation. Solving the transport equation jointly with the electrostatic problem for a finite 2DES, we determine a stability condition which includes conductivity, diffusion coefficient, and the system size.

Further, we allow for a non-zero difference between the work functions of two contacts to 2DES (leads), that gives rise to the photogalvanic effects in an irradiated sample¹⁷. We explore the distribution of the electrostatic potential and the electron density in such a sample for different values of the conductivity. Most remarkably, we find that in the diffusion-stabilized regime of negative conductivity the system splits into two regions with opposite directions of electric field. We argue that this effect is a precursor of the domain structure that is expected to emerge spontaneously in microwave-induced ZRS.

II. MODEL AND BASIC RESULTS

A. Microscopic conductivity and diffusion coefficient

The local dissipative current density in a weakly non-uniform 2DES with surface electron density n_s has a form

$$j = -2\sigma\nabla_s\phi|_{z=0} - eD\nabla_s n_s, \quad (1)$$

where $\phi|_{z=0}$ is the electrical potential in the 2DES plane $z = 0$, ∇_s is the surface gradient in this plane, σ is the

dissipative component of the magnetoconductivity tensor (per spin), and D is the diffusion coefficient.

In equilibrium, the conductivity σ_0 and the diffusion coefficient D_0 obey the Einstein relation $2\sigma_0 = e^2\chi D_0$, where $\chi = \partial n_s / \partial \mu$ is the equilibrium static compressibility (here μ is the 2DES chemical potential). The Einstein relation guarantees that $j = -2\sigma \nabla_s \eta / e$ is zero in the equilibrium state with constant electrochemical potential $\eta = e\phi|_{z=0} + \mu$; further, the current response does not depend on the type of perturbation (electric field or density gradient).

In the presence of microwaves the Einstein relation is violated,^{17,18}

$$2\sigma \neq e^2\chi D. \quad (2)$$

This violation leads to the photogalvanic effects observed experimentally in Refs. 15,22 and is at the heart of the phenomena discussed in the present work.

We start with demonstration that the theory¹⁷ allows for coexistence of a negative dissipative conductivity and a positive diffusion coefficient. This result is the most prominent for the case when effect of the microwave radiation on the electron kinetics is governed by modification of the electron distribution function (inelastic mechanism).¹⁹ For this mechanism, equations for the conductivity σ and the diffusion coefficient D read

$$\sigma = -\sigma_D \int \frac{\nu^2(\varepsilon)}{\nu_0^2} \frac{\partial f(\varepsilon)}{\partial \varepsilon} d\varepsilon, \quad (3)$$

$$D = \frac{2\sigma_D}{e^2} \int \frac{\nu^2(\varepsilon)}{\nu_0^2} \frac{\partial f(\varepsilon)}{\partial n_s} d\varepsilon. \quad (4)$$

Here $\sigma_D = n_s e^2 / 2m^* \omega_c^2 \tau$ is the Drude conductivity in a classically strong magnetic field, $\omega_c \tau \gg 1$; m^* is the effective mass, ω_c the cyclotron frequency, and τ the transport relaxation time. We remind the reader that at $\omega_c \tau \gg 1$ the dissipative resistivity is proportional to σ (since the dominant component of the conductivity tensor is the Hall conductivity that is only weakly affected by microwaves). Further, $\nu(\varepsilon)$ is the density of states in disorder-broadened Landau levels and $\nu_0 = m^* / 2\pi \hbar^2$ is the density of states per spin at $B = 0$. The non-equilibrium distribution function $f(\varepsilon)$ is determined by the kinetic equation.¹¹ Figure 1 illustrates the magnetic-field dependence of the dissipative conductivity σ and of the diffusion coefficient D for typical parameters. (Details of numerical procedure used for calculation of density of states $\nu(\varepsilon)$ and nonequilibrium distribution function $f(\varepsilon)$ are given in Ref. 21.) Under microwave radiation with the circular frequency ω , σ shows strong magnetooscillations (with periodicity controlled by the ratio ω/ω_c) and becomes negative around minima. At the same time, D remains almost unaffected by microwaves (apart from Shubnikov–de Haas oscillations that are strongly suppressed due to temperature smearing; for parameters in Fig. 1 their amplitude remains within 1%).

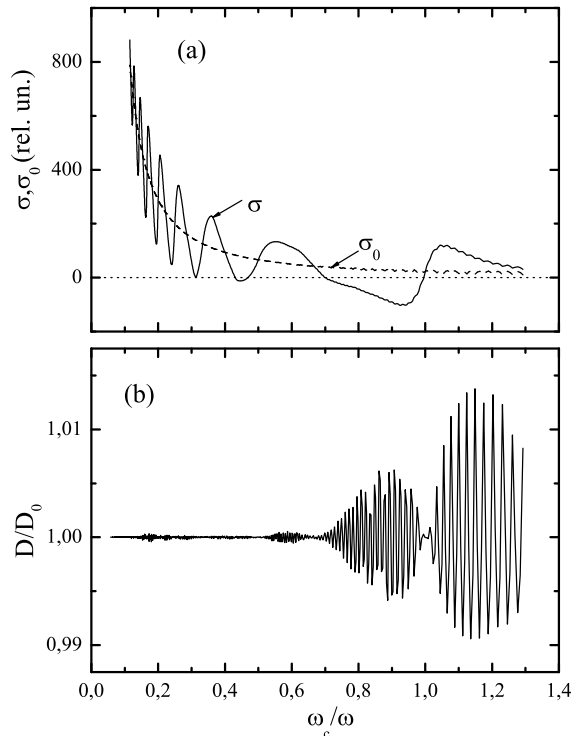


FIG. 1: Magnetic-field dependence of (a) the dissipative conductivity σ_0 , σ and (b) the normalized electron diffusion coefficient D/D_0 , shown as a function of the ratio ω_c/ω , where ω_c is the electron cyclotron frequency and ω is the circular radiation frequency. The quantities σ_0 and D_0 correspond to the dark conditions, while σ and D were calculated for a nonequilibrium state under microwave radiation. Parameters of calculations: electron surface density n_s corresponds to the filling factor of the Landau levels $N \approx 100$ at $\omega_c/\omega = 1$, $kT/\hbar\omega = 0.2$, and $\omega\tau_q = 10$. Here T is the dark temperature of 2DES and τ_q is the quantum scattering time determining the Landau level broadening.

B. Electrostatics and transport in a 2D stripe

We proceed now by finding a self-consistent solution of electrostatic and transport problems in a sample of finite length L subjected to microwave radiation and dc electric field. The considered geometry is shown in Fig. 2. Specifically, we assume that 2DES forms a stripe in the (x, y) plane between two infinite metal plates at $x = 0$ and $x = L$ which model Ohmic contacts. The magnetic field B is parallel to the z axis. In order to find a stationary spatial distribution of the 2D electron density $n_s(x)$ and of the potential $\phi(x, z)$ we use a system of coupled equations that includes the transport equation (1), the continuity equation

$$e\dot{n}_s + \nabla_s \cdot \mathbf{j} = 0, \quad (5)$$

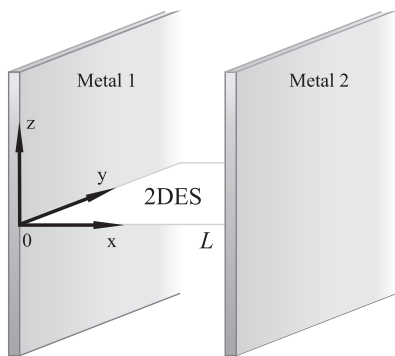


FIG. 2: Schematic view of the 2DES and metal contacts for considered electrostatic problem.

and the Poisson equation

$$-\epsilon\Delta\phi(x, z) = 4\pi e(n_s - n_+)\delta(z). \quad (6)$$

Here ϵ is the dielectric constant of the medium surrounding 2DES, and a constant n_+ represents the frozen positive background charge of ionized donors. In the bulk of an infinite sample, the electroneutrality requires $n_s = n_+$. In what follows, we assume that relative density variations are weak, $n_s - n_+ \ll n_+$, which allows us to use spatially-independent σ and D in Eq. (1). For simplicity, the system is assumed to be infinite in y direction. This setup can be termed “quasi-Corbino”, with x axis corresponding to the radial direction and y to the azimuthal direction of the Corbino disk. By symmetry, $n_s(x)$ and $\phi(x, z)$ do not depend on y , and the dissipative current (1) flows parallel to x -direction. The local density and electric field define the Hall component $j_y(x) = en(x)v_D(x)$, a dissipationless flow in y -direction with local drift velocity $v_D = -(c/B)\partial\phi(x, 0)/\partial x$.

The above equations are supplemented by boundary conditions for the electrostatic potential,

$$\phi(0, z) = \phi_0, \quad \phi(L, z) = 0, \quad (7)$$

$$(\partial\phi/\partial z)_{z\rightarrow\pm\infty} \rightarrow 0, \quad (8)$$

and for the density,

$$n_s(L) = n_+, \quad n_s(0) = n_+ - \chi e\mathcal{U}_c. \quad (9)$$

In Eq. (9), $e\mathcal{U}_c$ is the difference of work functions between the left lead and 2DES. Due to large density of states in the metallic lead, the interface charge density in 2DES $e(n_s(0) - n_+)$ is fixed by $e\mathcal{U}_c$ and is not affected by either the radiation or the current flow (see Ref. 17 for details). For simplicity, we assume that the right lead has the same work function as 2DES, so that $n_s(L) = n_+$. As we show below, a finite $e\mathcal{U}_c \neq 0$ makes the electrostatic problem nontrivial by introducing the spatial variation of the density n_s . Integrating Eq. (1) over x from 0 to L , we get a relation between the current density j , the electrostatic potential difference ϕ_0 , and the chemical potential difference $e\mathcal{U}_c$,¹⁷

$$jL = 2\sigma\phi_0 - e^2\chi D\mathcal{U}_c. \quad (10)$$

In the absence of 2DES ($n_s - n_+ = 0$) the Poisson equation (6) has a trivial solution $\phi(x, z) = \phi_0(1 - x/L)$. Splitting this contribution and expanding the remaining part in eigenfunctions of the Laplace operator with proper boundary conditions [Eqs. (7) and (8) with $\phi_0 = 0$], we get

$$\phi(x, z) = \phi_0 \left(1 - \frac{x}{L}\right) + \sum_{k=1}^{\infty} A_k e^{-k\pi|z|/L} \sin \frac{k\pi x}{L}. \quad (11)$$

With the use of Eq. (6), the charge density can be expressed in terms of coefficients A_k as follows:

$$e(n_s(x) - n_+) = \sum_{k=1}^{\infty} \frac{\epsilon k}{2L} A_k \sin \frac{\pi k x}{L}. \quad (12)$$

We integrate now Eq. (1) from x to L ,

$$j(L - x) = 2\sigma\phi(x, 0) + eD[n_s(x) - n_+], \quad (13)$$

and substitute here Eqs. (11) and (12). Using

$$1 - \frac{x}{L} = \frac{2}{\pi} \sum_{k=1}^{\infty} k^{-1} \sin \frac{\pi k x}{L}, \quad (14)$$

we finally obtain the coefficients A_k governing the stationary solution of the problem:

$$A_k = -\frac{4L}{\pi\epsilon k} \frac{e^2\chi\mathcal{U}_c}{k + L/\pi\lambda}. \quad (15)$$

Here we employed the relation (10) and introduced the non-equilibrium screening length

$$\lambda = \frac{\epsilon D}{4\pi\sigma} \quad (16)$$

(discussed in more detail below).

C. Nonequilibrium screening length

The nonequilibrium screening length (16) which enters the solution (15), plays a central role in nonequilibrium transport in inhomogeneous 2DES. In equilibrium (in the absence of microwaves), the Einstein relation holds and λ reduces to the conventional 2D Thomas-Fermi screening length,

$$\lambda \rightarrow \lambda_0 = \frac{\epsilon}{2\pi e^2\chi}, \quad 2\sigma_0 = e^2\chi D_0. \quad (17)$$

Using Eqs. (1), (5), and (6), it is easy to show that indeed λ replaces the equilibrium λ_0 in all electrostatic problems. Under microwave radiation, the local conductivity σ in Eq. (16) can cross zero and become negative, as illustrated in Fig. 1. The screening length λ diverges at $\sigma = 0$. As we show below, in the regime $\sigma < 0$ the stationary solutions of the linear problem become electrically unstable on the spatial scale $|\lambda|$ determined by the nonequilibrium screening length.

D. Stability conditions: finite-size effects

We check now the stability of the obtained solution with respect to slow spatio-temporal fluctuations. To this end, we add a fluctuating part \tilde{n} , $\tilde{\phi}$ and \tilde{j} to n_s , ϕ , and j . To satisfy the boundary conditions $\{\tilde{n}, \tilde{\phi}\}|_{x=0,L} = 0$, we take

$$\tilde{n}(x, y, t) = \delta n_q(t) e^{iq_y y} \sin q_x x \quad (18)$$

with $q_x = \pi k/L$, $k = 1, 2, \dots$, and continuous q_y . Using Eq. (6), the corresponding

$$\tilde{\phi}(x, y, z, t) = \frac{2\pi e}{\epsilon q} \delta n_q(t) e^{iq_y y - q|z|} \sin q_x x, \quad (19)$$

where $q = (q_x^2 + q_y^2)^{1/2}$. The fluctuating part of the current is therefore

$$\tilde{j} = -2\sigma \nabla_s \tilde{\phi}|_{z=0} - eD \nabla_s \tilde{n} - 2\sigma_H \hat{\epsilon} \nabla_s \tilde{\phi}|_{z=0}, \quad (20)$$

where we added to Eq. (1) the Hall term with $\sigma_H = en_s c/B$ and $\epsilon_{xy} = -\epsilon_{yx} = 1$. The continuity equation (5) gives

$$\frac{\partial \tilde{n}}{\partial t} = \frac{2\sigma}{e} \Delta_s \tilde{\phi}|_{z=0} + D \Delta_s \tilde{n} = - \left(\frac{4\pi\sigma}{\epsilon q} + D \right) q^2 \tilde{n}. \quad (21)$$

(The Hall term drops out since $\nabla_s \hat{\epsilon} \nabla_s \tilde{\phi} = 0$.) Therefore, fluctuations do not grow in time if the stability condition

$$\lambda^{-1} + q > 0 \quad (22)$$

is satisfied. The condition is most restrictive for soft modes with small q . In an infinite system, where perturbations at arbitrarily long spatial scale q^{-1} are possible, the condition (22) reduces to the usual one: $\lambda > 0$ or, equivalently, $\sigma > 0$.¹² In any finite system, q^{-1} is limited by the system size, and instability threshold shifts to negative σ . In particular, in 2D stripe of width L , the minimal wavenumber $q = \pi/L$ corresponds to the lowest harmonics $k = 1$ in Eqs. (11)-(15), and the stability condition (22) reads

$$L/\pi\lambda > -1, \quad (23)$$

or, equivalently,

$$\sigma > -\epsilon D/4L. \quad (24)$$

III. ANALYSIS OF RESULTS

In this section we discuss the obtained result (15) for the field (11) and density (12) distribution in different physical situations.

A. Homogeneous stable state with negative conductivity

In the plain-capacitor contact configuration, Fig. 2, and for vanishing difference of the contact work functions, $\mathcal{U}_c = 0$, all harmonics $A_k = 0$, see Eq. (15). The electron density (12) in initially homogeneous 2DES remains constant, $n_s = n_+$, independent on external bias $eV \equiv \eta(0) - \eta(L) = e\phi(0) - e\phi(L)$, and $\phi(x, z) = V(1 - x/L)$, see Eq. (11). The dissipative current (1) reduces to

$$j = 2\sigma V/L, \quad (25)$$

where σ manifests the microwave-induced oscillations illustrated in Fig. 1a.

In the finite system, the result (25) holds even for negative conductivity values, as long as the stability condition (24) is satisfied. Our analysis in Sec. IID shows that diffusion with $D > 0$ can stabilize otherwise unstable¹² homogeneous state with $\sigma < 0$ in a finite 2DES. According to Eq. (23), the lowest observable value of negative conductivity in a stable homogeneous state is

$$\sigma_c = -\epsilon D/4L \simeq -\pi\lambda_0\sigma_0/L, \quad (26)$$

where in the last equality we used $D \simeq D_0$ and Eq. (17); the subscript 0 refers to the dark equilibrium state. The critical value σ_c corresponds to the critical value $\lambda_c^{-1} = -\pi/L$ of the inverse nonequilibrium screening length (16) fixed by the lowest possible wavevector in the system.

At $\sigma < \sigma_c < 0$, the system becomes electrically unstable and breaks into domains. Possible domain configurations and their dynamics were addressed in Refs. 23–26. The appearance of electric domains implies an accumulation of charge at the boundary between domains of opposite polarity (domain walls). The nonequilibrium screening length sets the spatial scale of modulation of electronic density and electrostatic potential in the domain phase. Therefore, a proper account for the violated Einstein relation is crucial for understanding the critical properties of the nonequilibrium phase transition to ZRS, the microscopic structure of the domain walls, their dynamics, and sensitivity to boundary conditions and details of the disorder potential.

It should be mentioned that a negative residual conductivity has also been found in Ref. 23. Specifically, that work considered the domain phase ($\sigma < \sigma_c$ in our terminology) and obtained an exponentially small negative residual conductivity. We believe that the exponential dependence found in Ref. 23 is most likely an artefact of local electrostatic approximation used in Refs. 23–26. Such an approximation is appropriate for description of, e.g., the Gunn effect in bulk 3D semiconductors, but is not directly applicable to 2DES with quantized motion in z -direction. In contrast to 3D geometry, in 2D the relation between ϕ and n_s is non-local, see Eq. (6). For proper description of the domain phase, one should go beyond the linear response in Eq. (1). This regime requires development of adequate approaches for solution

of arising nonlinear nonlocal equations and will be addressed elsewhere.

B. Photogalvanic effects

We return now to an inhomogeneous system with a difference of work functions in 2DES and the left lead $e\mathcal{U}_c < 0$. For simplicity, we also assume that temperature is sufficiently high to suppress the magnetooscillations of the dark compressibility χ and Shubnikov-de Haas oscillations, $2\pi^2 kT/\hbar\omega_c \gg 1$. In this case, $D \simeq D_0$ (see Fig. 1b) and $\chi = \partial n_s/\partial\mu = n_s/\mu = 2\nu_0$, so that the electrochemical potential $\eta = e\phi|_{z=0} + n_s/2\nu_0$.

1. Current-voltage characteristics

The knowledge of spatial distributions (11) and (12) is not required for calculation of the current-voltage characteristics (CVC). Indeed, the CVC is given by the relation (10) which is obtained directly from Eq. (1) using boundary conditions (9). The electrostatic potential $\phi_0 \equiv \phi(0,0)$ can be expressed from Eqs. (7) and (9) in terms of electrochemical potential drop $eV \equiv \eta(0) - \eta(L)$ (measurable voltage across the sample) as $\phi_0 = V + \mathcal{U}_c$. Therefore, the CVC (10) reads

$$j = 2\sigma \frac{V}{L} + 2\sigma \frac{\mathcal{U}_c}{L} \left(1 - \frac{\lambda}{\lambda_0}\right). \quad (27)$$

The last term is responsible for photogalvanic effects. In the presence of contact asymmetry $\mathcal{U}_c \neq 0$ or other source of the built-in electric field \mathcal{U}_c/L and provided the Einstein relation is violated, $\lambda \neq \lambda_0$, the system displays photocurrent $j \neq 0$ at zero bias voltage $V = 0$, and photovoltage $V \neq 0$ at $j = 0$, see Ref. 17 for details. Our present results show that this characteristic stays valid for $\sigma < 0$ if the condition (23) is fulfilled. For the case of interest, $D > 0$, Eq.(27) predicts that both the differential resistance dV/dj and the photo-voltage $V_{\text{photo}} = \mathcal{U}_c(\lambda/\lambda_0 - 1)$ change sign when conductivity goes through the zero value. This prediction can be verified experimentally, e.g. on narrow Corbino disk samples which should behave similarly to the infinite stripe considered here. Importantly, the size of the sample L/λ_0 should not be very large in order to enable controllable measurements in the stable region (23) with $\sigma < 0$.

2. Field and density distributions

The charge and field distribution in the interior of the sample provides an additional insight into the problem and uncovers an interesting behavior in the vicinity of the instability threshold. Using Eqs. (11)-(15) and (27) we obtain the density profile

$$\frac{n_s(x) - n_+}{n_+ - n_s(0)} \equiv \frac{\mu(x) - \mu(L)}{e\mathcal{U}_c} = -\mathcal{N}\left(\frac{\pi x}{L}, \frac{L}{\pi\lambda}\right), \quad (28)$$

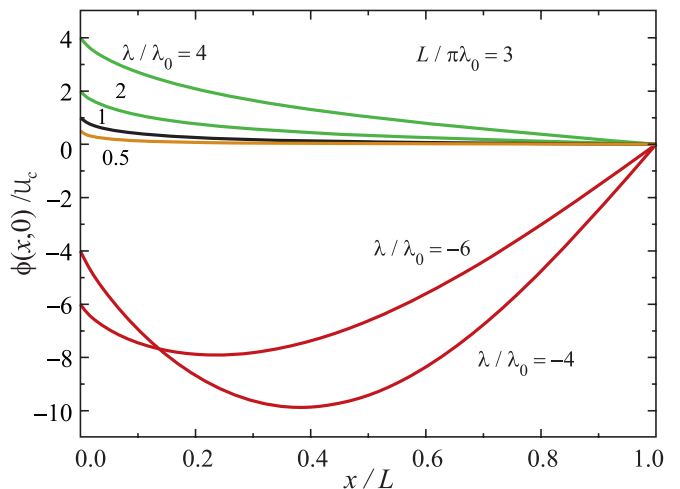


FIG. 3: The electrostatic potential $\phi(x,0)/\mathcal{U}_c$ vs. x/L for $j = 0$, $L = 3\pi\lambda_0$, and several different λ/λ_0 , see Eq. (31). Four upper curves correspond to $\sigma > 0$ ($\lambda > 0$). Two lower curves are calculated for $\sigma < 0$ satisfying the stability condition $L/\pi\lambda > -1$.

where

$$\mathcal{N}(X, \varkappa) = \frac{2}{\pi} \sum_{k=1}^{\infty} \frac{\sin kX}{k + \varkappa} = \frac{2}{\pi} \text{Im} \Phi(e^{iX}, 1, \varkappa), \quad (29)$$

and $\Phi(r, s, v) = \sum_{l=0}^{\infty} (v+l)^{-s} r^l$ is the Lerch transcendent. Further, the 3D electrostatic potential reads

$$\begin{aligned} \phi(x, z) &= (V + \mathcal{U}_c) \left(1 - \frac{x}{L}\right) \\ &- \frac{2L\mathcal{U}_c}{\pi^2\lambda_0} \sum_{k=1}^{\infty} \frac{\sin(\pi kx/L)}{k + L/\pi\lambda} \frac{e^{-\pi k|z|/L}}{k}. \end{aligned} \quad (30)$$

At $z = 0$, it can be represented as

$$\begin{aligned} \phi(x, 0) &= \left[V + \mathcal{U}_c \left(1 - \frac{\lambda}{\lambda_0}\right) \right] \left(1 - \frac{x}{L}\right) \\ &+ \mathcal{U}_c \frac{\lambda}{\lambda_0} \mathcal{N}\left(\frac{\pi x}{L}, \frac{L}{\pi\lambda}\right). \end{aligned} \quad (31)$$

Finally, the electrochemical potential

$$\begin{aligned} \eta(x) - \eta(L) &= eV \left(1 - \frac{x}{L}\right) \\ &+ e\mathcal{U}_c \left(1 - \frac{\lambda}{\lambda_0}\right) \left[1 - \frac{x}{L} - \mathcal{N}\left(\frac{\pi x}{L}, \frac{L}{\pi\lambda}\right) \right]. \end{aligned} \quad (32)$$

3. Enhancement of built-in field

Assuming an open circuit, $j = 0$, in Fig. 3 we show how the built-in electrostatic potential $\phi(x,0)$ is modified through the microwave-induced changes of the screening length λ . Equation (27) for the case $j = 0$ yields

$$\phi(0,0)/\mathcal{U}_c = V/\mathcal{U}_c + 1 = \lambda/\lambda_0 \simeq \sigma_0/\sigma. \quad (33)$$

In the last equality, we used $D \simeq D_0$. The electrostatic potential drop along the sample is enhanced at $0 < \sigma < \sigma_0$ (i.e. $\lambda/\lambda_0 > 1$), which is illustrated by two upper (green) curves in Fig. 3 (the colors in Fig. 3 and 4 refer to the online version). The black curve (third from above) illustrates the equilibrium distribution. In the case $\sigma > \sigma_0$ (orange curve $\lambda/\lambda_0 = 0.5$ in Fig. 3), the potential drop diminishes with respect to the equilibrium case. This behavior at $\sigma > 0$ illustrates the enhancement ($\sigma < \sigma_0$) and suppression ($\sigma > \sigma_0$) of the built-in electric field proposed for interpretation of photogalvanic effects in Ref. 22 on the experimental basis.

At $\sigma \rightarrow 0$, the potential $\phi_0 \equiv \phi(0,0)$ diverges in an open circuit, (namely, $\phi_0 \rightarrow +\infty$ at $\sigma \rightarrow +0$ and $\phi_0 \rightarrow -\infty$ at $\sigma \rightarrow -0$). This divergence is cut by nonlinear corrections to σ and D which are not taken into account here.²⁷ At $\sigma < 0$ and $j = 0$, illustrated by two lowest (red) curves in Fig. 3, the potential $\phi(x,0)$ develops a single minimum which approaches the position $x = L/2$ when σ approaches the critical value $\sigma_c = -\pi\lambda_0\sigma_0/L$, Eq. (26). In Fig. 3 we took $L = 3\pi\lambda_0$, so the corresponding critical value of λ is $\lambda_c = -L/\pi = -3\lambda_0$.

4. Analysis of the field and density distributions in different regimes

In an open circuit, $j = 0$, illustrated in Fig. 3, linear terms $\propto (1 - x/L)$ in (31) and (32) cancel out [see Eq. (27)]. Therefore,

$$\begin{aligned} \frac{\mu(x) - \mu(L)}{-e\mathcal{U}_c} &= \mathcal{N}\left(\frac{\pi x}{L}, \frac{L}{\pi\lambda}\right) = \frac{\lambda_0}{\mathcal{U}_c\lambda}\phi(x,0) \\ &= \frac{\eta(x) - \eta(L)}{(\lambda/\lambda_0 - 1)e\mathcal{U}_c}, \quad j = 0. \end{aligned} \quad (34)$$

General behavior (including $j \neq 0$) is illustrated in Fig. 4, where we subtract the linear term $\propto V(1 - x/L)$ in Eqs. (31) and (32). The rest, expressed in units \mathcal{U}_c , is fully determined by two parameters $L/\pi\lambda$ and λ/λ_0 . The relation between j and V for an arbitrary measurement scheme follows from CVC (27).

Several parametric regions deserve special attention.

(i) Continuous limit $\lambda \ll L$. This limit of strong screening is illustrated by three upper curves (green and black) in Figs. 4a, b, and c. In the region $x, \lambda \ll L$, the summation in Eq. (29) can be replaced by integration,

$$\begin{aligned} \mathcal{N}\left(\frac{\pi x}{L}, \frac{L}{\pi\lambda}\right) &\simeq \frac{2}{\pi} \int_{x/\lambda}^{\infty} \frac{dt}{t} \sin\left(t - \frac{x}{\lambda}\right) \\ &= \frac{2}{\pi} \text{ci} \frac{x}{\lambda} \sin \frac{x}{\lambda} - \frac{2}{\pi} \text{si} \frac{x}{\lambda} \cos \frac{x}{\lambda}, \quad \lambda, x \ll L. \end{aligned} \quad (35)$$

Here si and ci are the integral sine and cosine defined by $\text{ci}(z) + i \text{si}(z) = -\int_z^{\infty} (e^{it}/t) dt$. Similar distribution was obtained in Ref. 28 for equilibrium semi-infinite 2DES

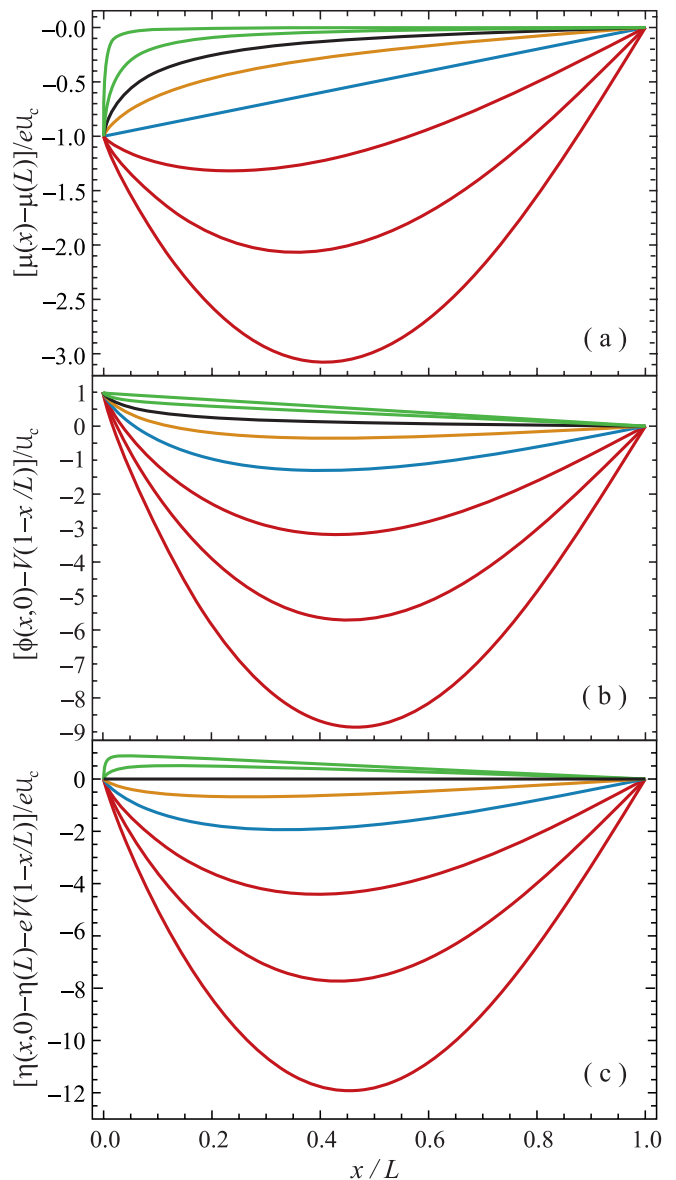


FIG. 4: Spatial distribution of (a) charge density, $[\mu(x) - \mu(L)]/e\mathcal{U}_c$ vs. x/L , Eq. (28); (b) the electrostatic potential, $[\phi(x,0) - V(1 - x/L)]/\mathcal{U}_c$ vs. x/L , Eq. (31); and (c) the electrochemical potential, $[\eta(x) - \eta(L) - eV(1 - x/L)]/e\mathcal{U}_c$ vs. x/L , Eq. (32). In (b) and (c) $L = 3\pi\lambda_0$ as in Fig. 3. The parameter $L/\pi\lambda = \{100, 10, 3, 1, 0, -0.5, -0.7, -0.8\}$ from top to bottom.

with different boundary conditions at $B = 0$. At large distances, Eq. (35) produces a power-law decay,

$$\mathcal{N} \simeq 2\lambda/\pi x, \quad \lambda \ll x \ll L, \quad (36)$$

characteristic for 2D electrostatics.

(ii) Enhanced screening, $\lambda \ll \lambda_0$, see two upper (green) curves in Figs. 4a, b, and c. This case corresponds to the well developed maxima of the microwave-induced resistance oscillations, $\sigma \gg \sigma_0$. Beyond the screening length,

$x > \lambda$, both ϕ and η change linearly with x . The slope,

$$-\frac{\nabla_s \eta}{e} = -\nabla_s \phi(x, 0) = \frac{V + \mathcal{U}_c(1 - \lambda/\lambda_0)}{L} = \frac{j}{2\sigma}, \quad (37)$$

is given by Eqs. (31) and (32) with $\mathcal{N} \rightarrow 0$. The second (diffusion) term in Eq. (1) is relevant only in the narrow region $x < \lambda$, where $|\nabla_s \mu/e| \simeq |\nabla_s \phi|_{z=0} |\lambda_0/\lambda| \gg |\nabla_s \phi|_{z=0}$.

(iii) Equilibrium, $\lambda = \lambda_0$, see black curves (third from top) in Figs. 4a, b, and c. When $\mathcal{U}_c \neq 0$ but there is no microwave field ($\lambda = \lambda_0$), $\phi(x, 0)$ and $n_s(x)$ vary near the left contact on scale λ_0 , while the nonlinear part of $\eta(x)$ is zero. Since the Einstein relation holds, two terms in Eq. (1) combine into one, $j = -2\sigma \nabla_s \eta/e = -2e\nu_0 D \nabla_s \eta = 2\sigma_0 V/L$. In other words, two terms in Eq. (1) partially compensate each other such that $\nabla_s \eta = -eV/L$ remains constant in space despite both $\nabla_s n_s$ and $\nabla_s e\phi$ vary strongly with $x \leq \lambda_0$.

(iv) Diffusion dominated screening, $\lambda > \lambda_0$, see orange curves (fourth from top) in Figs. 4a, b, and c. In this regime, diffusion dominates in the sense $e^2 \chi D > 2\sigma$. The nonequilibrium screening charge distribution [which is smooth compared to the equilibrium case (iii)] produces an ‘‘overshoot’’ in $\phi(x, 0)$: two regions with the opposite orientation of induced electric field appear, Fig. 4b (the total field may not change sign if the external voltage is sufficiently large). The corresponding nonequilibrium correction to η , Fig. 4c, changes sign and remains negative at $\lambda^{-1} < \lambda_0^{-1}$ (including negative λ^{-1} , see below).

(v) Zero-conductivity state, $\lambda^{-1} = 0$, see blue curves (fourth from bottom) in Figs. 4a, b, and c. In the limit $L \rightarrow \infty$, homogeneous state of 2DES becomes electrically unstable at $\lambda^{-1} = 0$.¹² In the finite system, the instability threshold shifts to negative σ determined by the condition $L/\pi\lambda = -1$.

As was discussed in Sec. IIIB3, in an open circuit, $j = 0$, the electrostatic potential $\phi(0, 0)$ has a singularity at $\sigma = 0$, which implies the necessity to include the non-linear effects. This divergence does not appear if one fixes the voltage V instead of current. Indeed, Eq. (1) with $\sigma = 0$ and boundary condition (9) yields the charge density varying linearly with x , $\mathcal{N} = 1 - x/L$, see Fig. 4a. The corresponding current density (1) has a V -independent value

$$j_s = eD(n_0 - n_+)/L = -\chi e^2 D \mathcal{U}_c \quad (38)$$

fixed by the boundary conditions. The voltage V decouples and can be arbitrary within the range where the linear-response approximation (1) is justified.

At $\lambda^{-1} = 0$, second term in Eq. (32) (which contains an indeterminate form of the type $\infty \cdot 0$) can be represented as

$$\frac{\eta(x) - \eta(L) - eV \left(1 - \frac{x}{L}\right)}{e\mathcal{U}_c} = \frac{2L}{\pi^2 \lambda_0} \text{Im Li}_2(e^{i\pi x/L}), \quad (39)$$

see Fig. 4c. Here we used $\sum_{k=1}^{\infty} k^{-2} \sin \frac{\pi k x}{L} = \text{Im Li}_2(\exp[i\pi x/L])$, where $\text{Li}_2(z)$ is the dilogarithm func-

tion. The potential profile induced by the linear variation of charge density $\mathcal{N} = 1 - x/L$ is $e\phi(x, 0) = \eta(x) - \eta(L) + e\mathcal{U}_c(1 - x/L)$, Fig. 4b.

(vi) Stable negative conductivity state, $-\pi/L < \lambda^{-1} < 0$, see three lowest (red) curves in Figs. 4a, b, and c. The distributions (28), (31), and (32) are dominated by first harmonics in Eq. (29),

$$\mathcal{N} \left(\frac{\pi x}{L}, \frac{L}{\pi \lambda} \right) \simeq \frac{2}{\pi} \frac{\sin(\pi x/L)}{1 + L/\pi \lambda}, \quad (40)$$

which diverges at the instability threshold, $1 + L/\pi \lambda = 0$.

5. Towards the domain structure

The divergence of our solution at the threshold $\lambda = -L/\pi$ signals an instability and transition to the domain phase. We believe that inclusion of nonlinear effects (in particular, taking into account dependence of σ entering Eq. (1) on the electric field $\nabla_s \phi$) should make the theory applicable also in the domain regime $1 + L/\pi \lambda < 0$. Work in this direction is currently underway.

Let us emphasize the emergence of a nonmonotonous profile of the electrostatic potential [see Figs. 3 and 4(b)] implying formation of two regions with opposite directions of the electric field. In our solution, the direction of electric field (+- vs. -+) in these two regions is determined by the sign of \mathcal{U}_c . A non-zero \mathcal{U}_c explicitly breaks the inversion symmetry $L/2 + x \leftrightarrow L/2 - x$. We argue that this effect which emerges at $\lambda < 0$ and grows while the system approaches the instability threshold, is the precursor of the domain structure which fully develops at $\lambda^{-1} < -\pi/L$. As was discussed in Sec. III A, in the homogeneous case $\mathcal{U}_c = 0$ the inversion symmetry is preserved at $\sigma_c < \sigma < 0$ and gets spontaneously broken at the instability threshold $\sigma_c = \sigma$.

A further important direction for future work is to go beyond the mean field approximation and to study the effects of fluctuations and noise on the transition into the ZRS regime. It is expected that field-theoretical approaches developed for nonequilibrium phase transitions, in particular, Martin-Siggia-Rose formalism, will be useful in this respect. First steps in this direction were made in Ref. 25.

IV. SUMMARY

In summary, the effect of the microwave radiation on the electron energy distribution function of a 2DES causes giant magneto-oscillations of the conductivity relative to its dark value and practically does not alter the electron diffusion coefficient. Such effect leads to magneto-oscillations of the photo-galvanic signals and of the screening length, which affects the potential profile in a sample. At the oscillation minima, the conductivity can become negative, which leads to a negative value of

the non-equilibrium screening length. We have derived the stability condition at which a finite 2DES can possess a stable state with a negative conductivity. When the conductivity becomes negative, the differential resistance and the photo-voltage also change their signs, which can be observed experimentally. We have further solved the combined transport and electrostatic problem and determined the profiles of the potential and the electron density inside the sample. In the stable state with a negative conductivity, the potential profile consists of

two regions with opposite directions of the electric field. The amplitude of these fields increases when the system approaches the instability threshold. This effect is a precursor of the domain structure in the regime of spontaneously broken symmetry.

This work was supported by the Deutsche Forschungsgemeinschaft and by the Russian Foundation for Basic Research. S.I.D. gratefully acknowledges fruitful discussions with Yu. A. Bychkov.

-
- ¹ M. A. Zudov, R. R. Du, J. A. Simmons, and J. L. Reno, Phys. Rev. B **64**, 201311(R) (2001).
- ² P. D. Ye, L. W. Engel, D. C. Tsui, J. A. Simmons, J. R. Wendt, G. A. Vawter, and J. L. Reno, Appl. Phys. Lett. **79**, 2193 (2001).
- ³ R. G. Mani, J. H. Smet, K. von Klitzing, V. Narayana-murti, W. B. Jonson, and V. Umansky, Nature **420**, 646 (2002).
- ⁴ M. A. Zudov, R. R. Du, L. N. Pfeiffer, and K. W. West, Phys. Rev. Lett. **90**, 046807 (2003).
- ⁵ C. L. Yang, M. A. Zudov, T. A. Knuuttila, R. R. Du, L. N. Pfeiffer, and K. W. West, Phys. Rev. Lett. **91**, 096803 (2003).
- ⁶ V. I. Ryzhii, Fizika Tverdogo Tela **11**, 2577 (1969) [Sov. Phys. Solid State **11**, 2078 (1970)].
- ⁷ A. C. Durst, S. Sachdev, N. Read, and S. M. Girvin, Phys. Rev. Lett., **91**, 086803 (2003).
- ⁸ M. G. Vavilov and I. L. Aleiner, Phys. Rev. B **69**, 035303 (2004).
- ⁹ S. I. Dorozhkin, Pis'ma v ZhETF **77**, 681 (2003) [JETP Lett. **77**, 577 (2003)].
- ¹⁰ I.A. Dmitriev, A.D. Mirlin, and D.G. Polyakov, Phys. Rev. Lett. **91**, 226802 (2003).
- ¹¹ I. A. Dmitriev, M. G. Vavilov, I. L. Aleiner, A. D. Mirlin, and D. G. Polyakov, Phys. Rev. B **71**, 115316 (2005).
- ¹² A. V. Andreev, I. L. Aleiner, and A. J. Millis, Phys. Rev. Lett. **91**, 056803 (2003).
- ¹³ A. L. Zakharov, Zh. Eksp. Teor. Fiz. **38**, 665 (1960) [Sov. Phys. JETP **11**, 478 (1960)].
- ¹⁴ V.L. Bonch-Bruевич, I.P. Zvyagin, and A.G. Mironov, *Domain electrical instabilities in semiconductors* (Consultants Bureau, New York, 1975); J.K. Pozhela, *Plasma and current instabilities in semiconductors* (Pergamon, Oxford, 1981); E. Schöll, *Nonlinear spatio-temporal dynamics and chaos in semiconductors* (Cambridge University Press, 2001).
- ¹⁵ R.L. Willett, L.N. Pfeiffer, and K.W. West, Phys. Rev. Lett. **93**, 026804 (2004).
- ¹⁶ S.I. Dorozhkin, L. Pfeiffer, K. West, K. von Klitzing, and J.H. Smet, Nature Physics **7**, 336 (2011).
- ¹⁷ I. A. Dmitriev, S. I. Dorozhkin, and A. D. Mirlin, Phys. Rev. B **80**, 125418 (2009).
- ¹⁸ A. Kashuba, Pisma v ZhETF **83**, 351 (2006) [JETP Lett. **83**, 293 (2006)].
- ¹⁹ The inelastic mechanism dominates over the displacement mechanism⁶⁻⁸ in the relevant domain of sufficiently low temperatures.^{11,20} The displacement mechanism produces additional contributions to σ and D , calculated in Ref. 17, and also violates the Einstein relation.
- ²⁰ I.A. Dmitriev, M. Khodas, A.D. Mirlin, D.G. Polyakov, and M.G. Vavilov, Phys. Rev. B **80**, 165327 (2009).
- ²¹ I. V. Pechenezhskii, S. I. Dorozhkin, and I. A. Dmitriev, Pis'ma v ZhETF **85**, 94 (2007) [JETP Lett. **85**, 86 (2007)].
- ²² S. I. Dorozhkin, I. V. Pechenezhskiy, L. N. Pfeiffer, K. W. West, V. Umansky, K. von Klitzing, and J. H. Smet, Phys. Rev. Lett. **102**, 036602 (2009).
- ²³ A. F. Volkov and V. V. Pavlovskii, Phys. Rev. B **69**, 125305 (2004).
- ²⁴ A. Auerbach, I. Finkler, B.I. Halperin, and A. Yacoby, Phys. Rev. Lett. **94**, 196801 (2005).
- ²⁵ J. Alicea, L. Balents, M.P.A. Fisher, A. Paramekanti, and L. Radzihovsky, Phys. Rev. B **71**, 235322 (2005).
- ²⁶ I. G. Finkler and B. I. Halperin, Phys. Rev. B **79**, 085315 (2009).
- ²⁷ In the linear approximation, the value $\sigma = 0$ dictates a definite value j_s of the current density j imposed by boundary conditions and independent of voltage V , see Eq. (38). Provided $j = j_s$, all potentials at $\sigma = 0$ remain finite.
- ²⁸ S. G. Petrosyan and A. Ya. Shik, Fiz. Tekh. Poluprovodn. **23**, 1113 (1989) [Sov. Phys. Semicond. **23**, 696 (1989)]; Zh. Eksp. Teor. Fiz. **96**, 2229 (1989) [Sov. Phys. JETP **69**, 1261 (1989)].